PHILOSOPHICAL TRANSACTIONS OF THE ROYAL SOCIETY A MATHEMATICAL, PHYSICAL & ENGINEERING SCIENCES

Apatite Fission Track Analysis: Geological Thermal History Analysis Based on a Three-Dimensional Random Process of Linear Radiation Damage

R. F. Galbraith, G. M. Laslett, P. F. Green and I. R. Duddy

Phil. Trans. R. Soc. Lond. A 1990 **332**, 419-438
doi: 10.1098/rsta.1990.0124

Apatite fission track analysis: geological thermal history analysis based on a three-dimensional random process of linear radiation damage

By R. F. Galbraith[1], G. M. Laslett[2], P. F. Green[3] and I. R. Duddy[3]

[1] *Department of Statistical Science, University College London, London WC1 E6BT, U.K.*

[2] *CSIRO DMS, Private Bag 10, Clayton 3168, Australia*

[3] *Geotrack International, P.O. Box 4120, Melbourne University, Victoria 3052, Australia*

Spontaneous fission of uranium atoms over geological time creates a random process of linearly shaped features (fission tracks) inside an apatite crystal. The theoretical distributions associated with this process are governed by the elapsed time and temperature history, but other factors are also reflected in empirical measurements as consequences of sampling by plane section and chemical etching. These include geometrical biases leading to over-representation of long tracks, the shape and orientation of host features when sampling totally confined tracks, and 'gaps' in heavily annealed tracks.

We study the estimation of geological parameters in the presence of these factors using measurements on both confined tracks and projected semi-tracks. Of particular interest is a history of sedimentation, uplift and erosion giving rise to a two-component mixture of tracks in which the parameters reflect the current temperature, the maximum temperature and the timing of uplift.

A full likelihood analysis based on all measured densities, lengths and orientations is feasible, but because some geometrical biases and measurement limitations are only partly understood it seems preferable to use conditional likelihoods given numbers and orientations of confined tracks.

1. Introduction

Figure 1 is a photograph of fission tracks in an apatite crystal. They are linear regions of damage about 10–20 μm long caused by spontaneous fission of ^{238}U atoms (trace uranium impurity incorporated into the apatite at crystallization). A plane interior surface, parallel to a prismatic face, has been polished and tracks intersecting it have been revealed by chemical etching. We call these *semi-tracks* because part of each original track (on average half) has been polished away. They have varying orientations and the dimensions seen in figure 1 are those of their projections onto the polished plane. There are also four fully *confined tracks*. A confined track may be revealed because it intersects a semi-track, the etchant having passed down the semi-track into the confined track; this is called a *tint* (track-in-track). Alternatively, a confined track may be revealed because it intersects a fracture in the crystal and thus has been etched; this is a *tincle* (track-in-cleavage). The four confined tracks in figure 1 are all tincles.

Phil. Trans. R. Soc. Lond. A (1990) **332**, 419–438
Printed in Great Britain

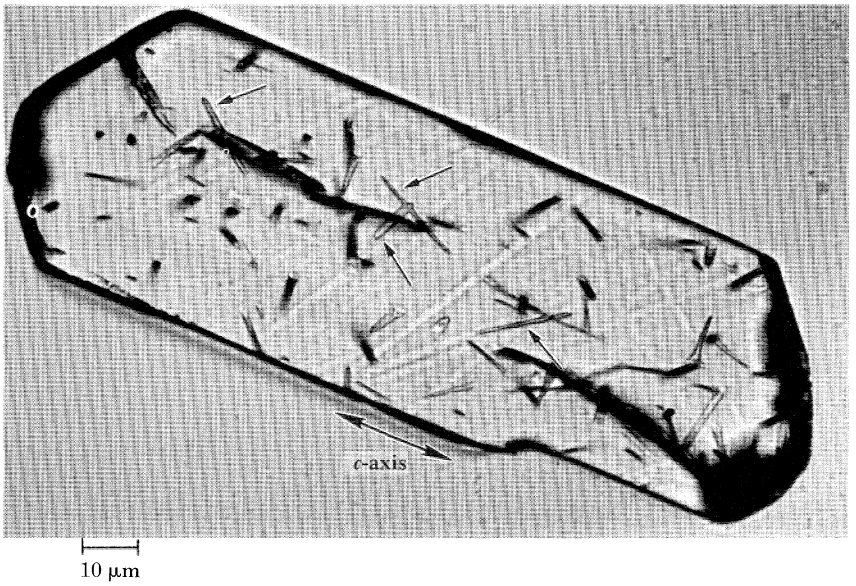

Figure 1. Fission tracks in apatite. Tracks intersecting a polished surface (i.e. semi-tracks) are revealed by chemical etching. The track openings are seen as light-coloured rectangular slots, and are aligned in the direction of the crystal's '*c*-axis'. Four totally confined tracks, indicated by arrows, have been etched because they intersect semi-tracks or fractures. The larger etched regions are fractures; the faint lines are polishing scratches. Photograph reproduced, with permission, from Gleadow *et al.* (1986).

The number of semi-tracks intersecting a surface depends on the concentration of uranium impurity and the time over which tracks have been forming, so if the former could be measured the latter might be deduced. This idea led to the development of *fission track dating* as a geochronological method. The number of tracks also depends on the amount of heating they have undergone, particularly in apatite at temperatures normally found in the upper few kilometres of the Earth's crust, and this affects the interpretation of the fission track age. More generally, because fission tracks accumulate over time, the statistical distribution of their number, lengths and orientations reflects the whole thermal history experienced by the host crystal. A central aim of this paper is to understand and quantify the information relating to thermal history that can be extracted from data such as in figure 1; in particular, how to combine information from measurements of track density, lengths and orientations of confined tracks, and lengths and orientations of projected semi-tracks.

In §2 we describe the mathematical basis of fission track dating, while §3 deals with annealing and the need to measure lengths; §4 is concerned with confined track measurements and some geometrical biases inherent in them, while in §5 we try to use projected semi-track lengths and orientations to estimate the timing and severity of a thermal event. Finally in §6 we discuss the combined likelihood function for all these measurements.

2. The mathematical basis of fission track dating

Originally, Price & Walker (1963) derived their fission track age equation using a deterministic argument. Here we give a stochastic argument to derive both the age equation and the statistical distributions associated with it.

A ^{238}U atom may either decay by α-emission after a random time D, or spontaneously fission after a random time S, where D is exponential with rate $\lambda = 1.55 \times 10^{-10}$ a^{-1}, S is exponential with rate $\lambda_f \approx 7 \times 10^{-17}$ a^{-1}, and S and D are independent. The probability that such an atom has spontaneously fissioned by time t is therefore:

$$p(t) = \Pr\{S \leqslant t, S \leqslant D\} = [\lambda_f/(\lambda_f+\lambda)]\{1-\exp[-(\lambda+\lambda_f)t]\}. \tag{1}$$

Since $p(t)$ must always be smaller than $\lambda_f/(\lambda_f+\lambda) \approx 5 \times 10^{-7}$, it is reasonable to regard the locations of the fissioned ^{238}U atoms in a crystal as a realization of a Poisson point process in three-dimensional space; the formal argument appeals to thinning theorems of point processes. The expected number of fissioned ^{238}U atoms per unit volume is $\tau = \tau_0 p(t)$, where τ_0 is the concentration of ^{238}U at the time of formation of the host crystal. If τ_c is the current concentration of ^{238}U, then

$$\tau_c = \tau_0 \Pr\{S > t, D > t\} = \tau_0 \exp[-(\lambda+\lambda_f)t]$$

so that

$$\tau/\tau_c = [\lambda_f/(\lambda_f+\lambda)]\{\exp[(\lambda+\lambda_f)t]-1\}. \tag{2}$$

Hence, if τ and τ_c could be measured, the age of the crystal t could be inferred.

Information about τ is obtained by counting tracks that intersect a polished planar surface within the body of the crystal. These tracks are formed before polishing, and arise from fissioned ^{238}U atoms on both sides of the surface. The expected number of such tracks may be calculated as follows. Assume that a track is a line-segment of random orientation (uniform solid angle) and length l having probability density $f(l)$ independent of orientation. Then, referring to the coordinate system in figure 2, (l, ϕ, θ) has probability density

$$(1/2\pi)\sin\phi f(l), \quad 0 < \theta < 2\pi, \quad 0 < \phi < \tfrac{1}{2}\pi, \quad 0 < l < \infty. \tag{3}$$

Let N be the number of tracks intersecting a unit square area in the yz plane. First, focus on tracks with a specific (l, ϕ, θ). If the centre of such a track falls within a parallelepiped of height $h = l \sin\phi|\cos\theta|$, it will intersect the square area. The number $N(l, \phi, \theta)$ of such tracks is obtained by multiplying the number per unit volume, $\tau \sin\phi \, d\phi f(l) \, dl \, d\theta/(2\pi)$, by the volume, which because the parallelepiped has a base area of unity, is equal to h. Integration over all (l, ϕ, θ) then leads to

$$\mathrm{E}[N] \equiv \rho = \tfrac{1}{2}\tau\mu, \tag{4}$$

where μ is the mean track length. The same style of argument leads to the conclusion that N must have a Poisson distribution: $N(l, \phi, \theta)$ is a volume count of the three-dimensional Poisson process of fissioned ^{238}U atoms with specific (l, ϕ, θ), so that N is the count from the superposition of independent Poisson processes.

Information about τ_c is obtained indirectly from $\tau_{235} = \beta\tau_c$, where τ_{235} is the current concentration of ^{235}U, and $\beta(=7.25 \times 10^{-3})$ is the ^{235}U:^{238}U isotopic ratio. Various approaches to measuring τ_{235} have been proposed, all of which involve irradiation of crystals with thermal neutrons, thus inducing a measurable proportion of ^{235}U to fission, and creating induced fission tracks. These include the population method, the re-etch method, the external surface method, and many variants. But

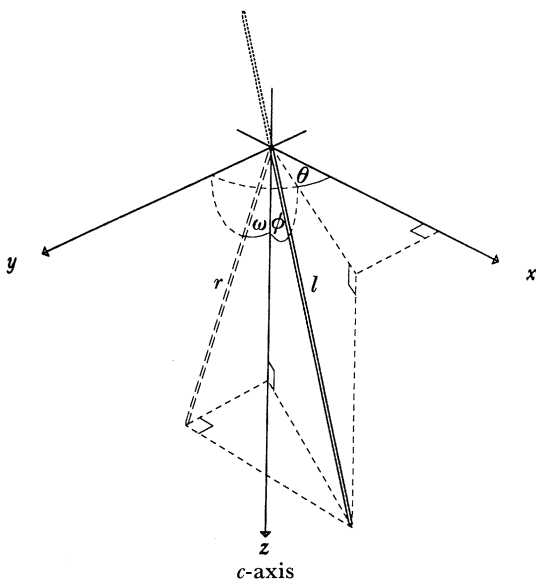

Figure 2. Coordinate axes showing track length l, projected semi-track length r, orientation angles ϕ and θ, and the angle ω between the projection of the track on the yz plane and the z-axis. The yz plane is the plane of observation; for apatite this is assumed to be a prismatic face, with the z-axis parallel to the crystallographic c-axis. The full length l cannot be observed, because only the solid part is within the crystal, the dotted part having been polished away.

the most popular and most useful for the dating of the common accessory mineral apatite is the *external detector method*, which we now describe.

After separation from the host rock, the apatite crystals are mounted in epoxy resin. The mount is polished to a smooth surface with aluminium oxide paste, exposing a flat interior surface of several crystals. Spontaneous tracks intersecting a polished surface are revealed by etching with 5 M HNO_3 for 20 s at 20 °C. A flat piece of mica (containing negligible uranium) is then clamped to the polished surface, and the whole mount is irradiated. Induced tracks near the surface may emerge from the apatite, and create linear regions of damage within the mica. The mica is then unclamped, and its tracks are also revealed by etching.

The expected number of fissioned ^{235}U atoms per unit volume is

$$\tau_i = \Phi\sigma\tau_{235} = \Phi\sigma\beta\tau_c,$$

where $\Phi\sigma$ is the probability that a ^{235}U atom will be fissioned, Φ being the thermal neutron fluence in number of neutrons per square centimetre and $\sigma(= 580.2 \times 10^{-24}\ \mathrm{cm}^2)$ being the microscopic fission cross section of ^{235}U. The density of induced tracks intersecting the mica surface is then given by

$$\rho_i = \tfrac{1}{4}\tau_i\mu_i = \tfrac{1}{4}\Phi\sigma\beta\tau_c\mu_i.$$

The factor $\frac{1}{2}$ in (4) becomes $\frac{1}{4}$ here, because the induced tracks arise just from ^{235}U atoms below the crystal surface.

Assuming $\mu_i = \mu$, substituting for τ and τ_c in (2) in terms of ρ and ρ_i and rearranging, leads to the fission track age equation

$$t = \frac{1}{\lambda + \lambda_f} \ln\left\{1 + \frac{\lambda + \lambda_f}{2\lambda_f}\beta\sigma\Phi\frac{\rho}{\rho_i}\right\}. \tag{5}$$

In practice, ρ and ρ_i are estimated from counts on matching areas of crystal and mica for each of several crystals. The thermal neutron fluence Φ is measured as $\Phi = B\rho_d$, where B is a calibration factor and ρ_d is the density of tracks induced in a standard uranium-bearing glass that was irradiated with the mount. Because of uncertainty about the values of λ_f and B, the modern approach is to use $\beta\sigma\Phi/\lambda_f = \zeta\rho_d$ in (5), where the calibration factor ζ is determined by dating samples of known age (Hurford & Green 1983).

A consequence of this model is that the numbers of spontaneous and induced tracks in matched areas A have independent Poisson distributions with means

$$\tfrac{1}{2}A\mu[\lambda_f/(\lambda_f+\lambda)]\{\exp[(\lambda+\lambda_f)t]-1\}\tau_c \quad \text{and} \quad \tfrac{1}{4}A\mu\beta\sigma\Phi\tau_c.$$

These means vary with τ_c, and of course with A, but their ratio depends only on t (Galbraith 1984). This model provides a sound basis for obtaining an age estimate and its precision for each crystal, as well as for several crystals combined, and for assessing heterogeneity between crystals. It is a feature of the external detector method that variation in uranium concentration between crystals, which is often considerable, does not contribute to variation in individual age estimates or to the error variance of the combined estimate.

3. Fission track analysis

3.1. *Fission track annealing*

Figure 3 displays two samples of apatite fission track age estimates: 20 crystals from an outcrop and 30 crystals from a depth of 2.6 km in a borehole nearby. The precision of each estimate is based on the model of §2 and allows only for Poisson variation in the numbers of spontaneous and induced tracks counted, along with a small amount of error (less than 2%) in measuring Φ.

The outcrop estimates are clearly consistent with each other and they agree with the age of deposition. Such homogeneity is typical of samples with a 'clean' thermal history: that is, rapid cooling from a high temperature to below about 50 °C and no subsequent heating, so the fission track age indicates the time of cooling.

The borehole estimates (figure 3) differ in two respects: they are generally younger than the depositional age and they are heterogeneous. These are consequences of thermal annealing, due to the higher temperature (currently *ca.* 92 °C) experienced at this depth. When fission tracks are heated they shorten and, at a sufficiently high temperature, disappear. Because their mean length μ is reduced, the age equation (5) will underestimate the original time of cooling (μ_i being unaffected). The heterogeneity is due to varying chemical composition between crystals, those with a higher F:Cl ratio being more sensitive to heat (Green *et al.* 1986).

It has therefore been found that geological interpretation is greatly clarified by measuring track lengths, initially to 'correct' fission track ages (Storzer & Wagner 1969), and more recently to provide additional information on thermal history (Gleadow *et al.* 1986). Thus because tracks form continuously over time, and the length of each shrinks to a value characteristic largely of the maximum temperature it experiences, the final length distribution reflects the variation of temperature with time.

What length measurements are available? The most abundant are projected semi-track lengths (r in figure 2). However, because of censoring and projection, the theoretical distribution of these is insensitive to the shape of the underlying length

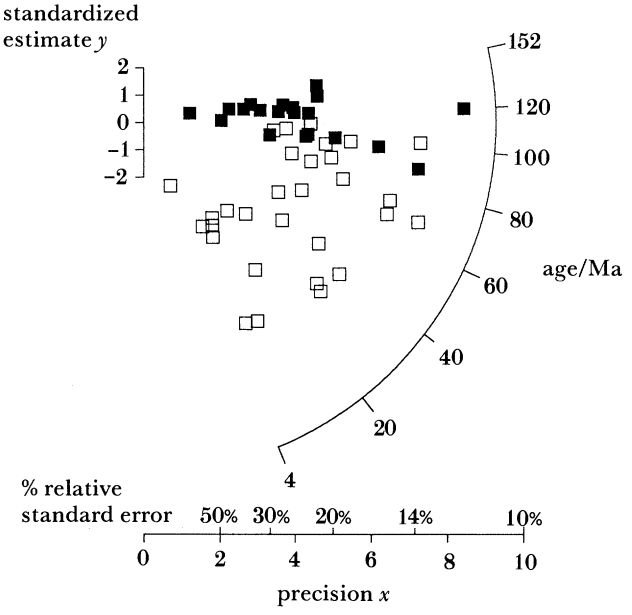

Figure 3. Radial plot (Galbraith 1988) of apatite fission track age estimates for 20 crystals from an outcrop, ■ (Barrabool Hills, Otway Ranges) and 30 crystals from a borehole, □ (Flaxmans-1, Otway Basin, depth 2.6 km). Each estimate has unit standard error on the y-scale, its actual precision is indicated on the x-scale and its age is indicated by extrapolating a line from $x = 0, y = 0$ through the plotted point. The outcrop estimates are clearly homogeneous; their pooled age (113 Ma, standard error (SE) 6 Ma) agrees with the depositional age (*ca.* 120 Ma, Gleadow & Duddy 1981). The borehole estimates are clearly heterogeneous, ranging from zero to the depositional age.

distribution. It is in principle possible to measure actual semi-track lengths, but this is considered impractical. Much more informative are lengths of horizontal confined tracks: tints and tincles that are parallel to the polished plane. Even these are subject to geometrical biases, which need to be understood to recover the true length distribution $f(l)$. We discuss such biases in §4.

3.2. *Characteristics of fission track annealing*

When a cohort of fresh fission tracks is heated, the tracks anneal and their mean length decreases. A quantitative description of how mean length depends on temperature and time has been derived from laboratory studies (Laslett *et al.* 1987; Duddy *et al.* 1988). But what happens to individual tracks? Green *et al.* (1986) showed that the dominant annealing mechanism is shrinkage from the ends inwards. A supplementary 'gapping' mechanism occurs only when there is heavy annealing (that is, at temperature–time combinations just below those causing the tracks to disappear completely), and in only a small proportion of etched tracks. Therefore, tracks seem to retain their linear shape under annealing.

Green & Durrani (1977) and Green (1981) reported that the length distribution of annealed tracks in apatite is anisotropic: tracks at a high angle to the c-axis tend to be shorter than tracks at a lower angle. For unannealed samples, the length distribution is nearly isotropic; as annealing progresses, not only does the mean length decrease, but also the anisotropy becomes more marked. To allow for

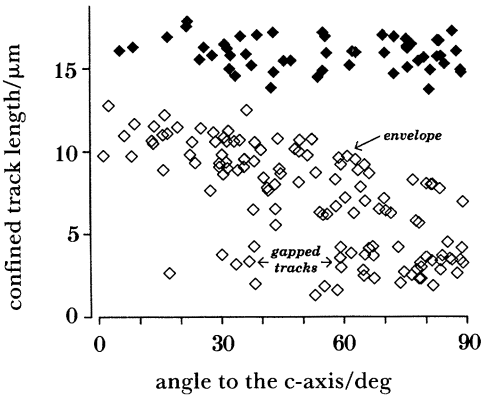

Figure 4. Scatterplot of measured lengths and angles to the *c*-axis for horizontal confined tracks in Durango apatite. Solid diamonds denote unannealed tracks; open diamonds denote tracks that have been annealed for 1 h at 343 °C. The annealed tracks have an anisotropic length distribution, and are of two types: non-gapped tracks, whose lengths make up an anisotropic 'envelope'; and very short gapped tracks. These data are discussed further in §4.1.2.

anisotropy, formula (3) for the probability density of (l, ϕ, θ) is modified by substituting f_ϕ, the conditional density function of length given orientation, in place of f, and (4) becomes

$$\rho = \tau \frac{2}{\pi} \int_0^{\frac{1}{2}\pi} \sin^2 \phi \mathrm{E}[l \,|\, \phi] \, \mathrm{d}\phi \tag{6}$$

(Laslett *et al.* 1984; Galbraith & Laslett 1988). It follows that track orientations are potentially informative. Measurements of ϕ are now made routinely for horizontal confined tracks and measurements of ω (figure 2) are made for semi-tracks.

These characteristics of annealing are illustrated in figure 4, which shows measured lengths and angles to the *c*-axis of horizontal confined tracks, some unannealed and some annealed for 1 h at 343 °C. The unannealed tracks have lengths in the range 14–18 μm, with a mean of about 16 μm, and little evidence of anisotropy. By contrast, the length distribution of the annealed tracks is distinctly anisotropic. The lengths are characterized by an annealing envelope, an upper bound to the annealed track length, which decreases with increasing angle to the *c*-axis. In addition, some tracks at high angles to the *c*-axis are gapped, and their lengths are much shorter than the maximum possible given by the envelope. Sequential etching experiments show that these tracks will attain lengths closer to the envelope with further etching (Green *et al.* 1986).

3.3. *Thermal histories and two-component mixtures*

Quite complex thermal histories can give rise to 'true' fission-track length distributions that are nearly two-component mixtures. One such situation is shown in figure 5: an apatite crystal of volcanic origin is deposited in a sediment and progressively buried as newer sediments accrue, then it is subjected to a relatively short period of uplift and erosion, after which it is progressively buried with further sedimentation. Temperature increases with depth of burial, so fission tracks present before uplift experience higher temperatures than those created after uplift. Because

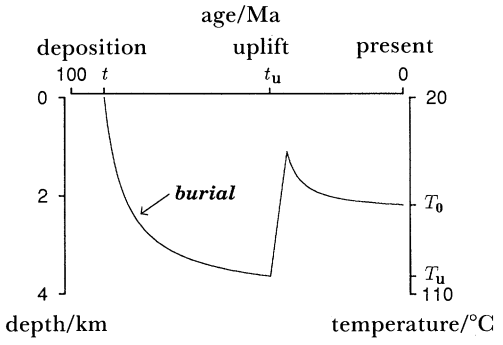

Figure 5. A schematic diagram of burial and uplift (and corresponding thermal history) of a sediment in which the source material is derived from volcanism. An apatite in this sediment will contain essentially a two-component mixture of fission track lengths.

tracks spend some time near their highest temperatures, their current length distribution will be effectively a two-component mixture, in which the parameters reflect the current temperature T_0, the maximum temperature T_u and the proportion of tracks formed before uplift. It is therefore of considerable interest to recover these parameters. The timing of uplift t_u and the total time t can then be inferred from information on densities, but realistically, the whole thermal history cannot be recovered from fission tracks (Green *et al.* 1989). (Note, incidentally, that in figure 1 there are three long tincles of roughly equal length and one short tincle of about half their length. This immediately suggests that the crystal may have experienced a thermal event sufficiently severe to halve a track's length and sufficiently long ago for several tracks to form since cooling.)

Of course, if the current temperature is too high no tracks will be found, and if the maximum temperature is too high, there will be no pre-uplift tracks and therefore no information about thermal history before uplift. Usually, a suite of samples downhole are available, and the parameters can be inferred by combining information from confined tracks appropriately across samples. Occasionally the samples contain few confined tracks and it is then worthwhile asking: would projected semi-track lengths and orientations provide useful additional information? We address this question in §5.

4. Biases in horizontal confined track measurements

4.1. *Length bias*

For a confined track to be etched and hence observed, it must intersect an etched fracture or semi-track (that is, be a tincle or tint). A uranium atom associated with a longer track can be further away from the fracture or host semi-track and still give rise to a tincle or tint. Hence longer tracks will be over-represented in a sample. Clearly the sampling bias factor is proportional to the volume of the region in which the etched track's associated uranium atom can lie, and hence (for a horizontal track) is proportional to the track's length. Under the isotropic line-segment model (3), Laslett *et al.* (1982) showed that the length distribution of horizontal tincles and tints has the length-biased density

$$g(l) = lf(l)/\mu,$$

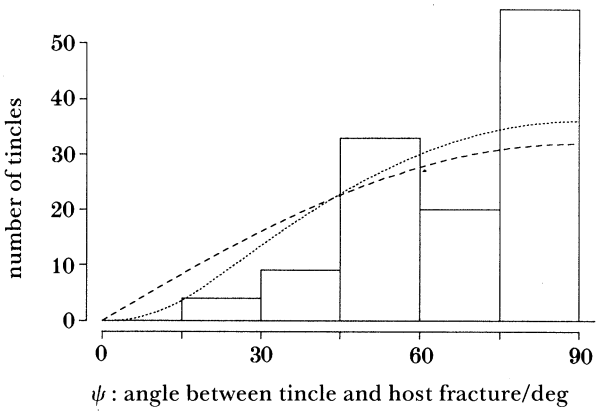

Figure 6. Histogram of the angles ψ of tincles to their host fractures for 122 unannealed tincles in Durango apatite. Ignoring fracture thickness, the histogram should conform to a sine curve. The effect of fracture thickness is to lessen the number of tincles at an acute angle to the fracture. The scaled PDFs are ——, sine curve; · · · · ·, corrected for fracture thickness.

whereas for non-horizontal tracks the bias is more complicated. Despite its sound theoretical basis, this principle needs empirical verification before it can be applied in practice with confidence. We discuss two methods of such verification.

4.1.1. *Angles of tincles to host fractures*

Evidence of length bias can be seen by examining the distribution of angles of unannealed horizontal tincles to their host fractures. A track of length l is more likely to intersect a fracture if its angle ψ to the fracture is higher (nearer 90° rather than nearer 0°). Treating the fracture as a vertical plane, it is easy to show that the joint density function of l and ψ for horizontal tincles is

$$l \sin \psi f(l)/\mu, \quad 0 < \psi < \tfrac{1}{2}\pi, \quad 0 < l < \infty.$$

(The geometry is essentially that of length bias, as outlined above: in effect, $l \sin \psi$ is the length-bias factor for tincles at angle ψ.) Thus for tracks that intersect the fracture, ψ is independent of l and has density $\sin \psi$, whereas for a true random sample of tracks ψ would be uniform. By concentrating on the distribution of ψ, we avoid the problem of not knowing $f(l)$.

Motivated by this argument, G. M. Laslett measured the length l, orientation ϕ, fracture width β and angle ψ for 122 tincles in Durango apatite. This sample is only lightly annealed, and was chosen to avoid problems with anisotropy of the length distribution. The frequency histogram of the ψ measurements (figure 6) departs markedly from a uniform distribution and broadly follows a sine curve; indeed, is even more biased towards high angles. In practice, an observer needs to see both ends of a track to be sure it is horizontal and fully confined, so he will only measure tincles with both ends showing. If the host fracture has thickness β, the expected number of such tracks is proportional to $l \sin \psi - \beta$, provided this quantity is positive (figure 7). Thus the conditional density of ψ given l and β for sampled tincles is

$$\frac{l \sin \psi - \beta}{l\{1-(\beta/l)^2\}^{\frac{1}{2}} - \beta\{\frac{1}{2}\pi - \arcsin(\beta/l)\}}, \quad \arcsin(\beta/l) < \psi < \tfrac{1}{2}\pi.$$

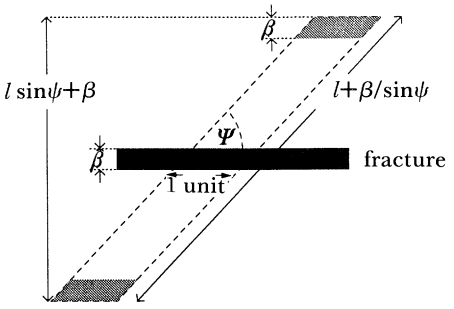

Figure 7. The diagram shows a horizontal cross-section of a parallelipiped of height $\beta + l \sin\psi$ intersecting a unit area of a fracture. If the centre of a horizontal track of length l at angle ψ to the fracture falls in the parallelipiped, a tincle will be created. But it will not be measured if its centre falls in either shaded region, for then one of its ends falls in the fracture. Hence the expected number of tincles (of length l and angle ψ) per unit area of the host fracture is proportional to the volume of the parallelipiped minus the shaded ends, $l \sin\psi - \beta$.

Summing this density function for each tincle (that is, for each measured l and β) and rescaling gives the curve 'corrected for fracture thickness' in figure 6, which is in better agreement with the data.

This analysis ignores other features encountered in making real measurements. Some fractures cast a shadow that may obscure a track end (particularly in transmitted light, although in our data both transmitted and reflected light were used). If the width of shadow is s, then the expected number of horizontal tincles with both ends showing is proportional to $l \sin\psi + \beta - 2s$, which reduces to the previous formula when $s = \beta$. Secondly, an observer needs to see enough of a tincle to measure it: if it is at an acute angle to the fracture, so that each end is just visible in theory, it still may not be measurable; indeed, it may be etched so as to merge with the fracture. On present evidence therefore, the effects of fracture thickness and measurement limitations can explain the observed departure from length-biased sampling.

The above argument assumes implicitly that fractures are formed after the fission tracks are created, and their formation does not alter the length of the intersecting tracks. Fractures, like tracks, are widened by etching, so that this assumption is at least partly correct. Other models of fracture formation would lead to different corrections for fracture thickness.

4.1.2. *Two-component mixtures*

Consider a two-component mixture of fission tracks with true length density

$$f(l) = (1-p) f_0(l) + p f_1(l),$$

where the density of long tracks f_0 has mean μ_0, f_1 has mean $\mu_1 < \mu_0$, and p is the proportion of uranium atoms (by volume) giving rise to tracks in the short component. Then the length-biased density $g(l)$ will also have two components, but with a smaller proportion q in the short component, where

$$q = p\mu_1 / [p\mu_1 + (1-p)\mu_0].$$

To test this theory, P. F. Green did some experiments as follows: ^{235}U atoms in ten

Table 1. *P. F. Green's experiments*

high fluence		low fluence	
D2	unannealed control	D13	unannealed control
D4	annealed control, 300 °C	D15	annealed control, 300 °C
D6	15:1 mixture of D4 and D2	D17	5:1 mixture of D15 and D13
D8	annealed control, 343 °C	D19	annealed control, 343 °C
D10	15:1 mixture of D8 and D2	D21	5:1 mixture of D19 and D13

Table 2. *Summary data from P. F. Green's mixture experiments*

	no. of tracks					
experiment	long	short	proportion short	SE	p	$\hat{q}$
D6	14	156	0.918	0.021	0.938	0.904
D10	23	83	0.783	0.040	0.938	0.852
D17	48	142	0.747	0.032	0.833	0.754
D21	52	128	0.711	0.034	0.833	0.676

samples of Durango apatite were induced to fission, five under a high fluence and five under a low fluence, and a sample of each was set aside as unannealed controls; the remaining eight samples were thermally annealed for 1 h at one of two temperatures (300 °C or 343 °C), and four annealed control samples were set aside. In the remaining four samples, further ^{235}U atoms were induced to fission to produce mixtures of annealed and unannealed tracks. The ten samples obtained are listed in table 1.

Figure 4 shows confined track data from experiment D21. In this and each of the other three mixtures it is very easy to allocate the tracks to each component, and the observed proportion of short tracks (table 2) is less than the nominal true proportion p. Table 2 also gives estimated values of q, which are in broad agreement with the observed proportions. (To estimate q, μ_0 was estimated using the approximate length-bias correction $\hat{\mu}_0 = \bar{y}_0 - s_0^2/\bar{y}_0$, where $\bar{y}_0$ and s_0 are the mean and standard deviation of the observed track lengths in the unannealed control, and μ_1 was similarly estimated from the annealed control.)

Of course, this comparison is over simple because the formula for q is based on the isotropic model, which is incorrect for annealed samples. Under the anisotropic model the length-biased density of l given ϕ is

$$g_\phi(l) = l f_\phi(l)/\mathrm{E}[l\,|\,\phi]$$

and the above theory applies at each angle ϕ. A slightly more refined comparison, made by grouping ϕ into three intervals (0°–40°, 40°–70°, 70°–90°) and assuming $\mathrm{E}[l\,|\,\phi]$ constant within each, shows that the observed proportion of short tracks decreases with increasing ϕ, in good agreement with $\hat{q}$. Thus we have considerable empirical evidence that a sampling bias exists, which is to a large extent explained by simple length bias.

Anisotropy has other consequences for the measurement of length distributions in annealed samples. For example, it means that the theoretical distribution functions for semi-track and projected semi-track lengths are not those given in Dakowski (1978) and Laslett *et al.* (1982). The modified theory is given by Galbraith & Laslett (1988).

4.2. *Orientation bias*

Table 3 gives the number of horizontal tints classified by angle ϕ to the c-axis for unannealed induced tracks in Durango apatite, and also for tracks annealed for one hour at one of several temperatures. Theory suggests that the number of tracks should be uniformly distributed with respect to ϕ (or be biased towards low angles because of length-biased sampling), but the data clearly depart from this.

A possible reason is the shape of host semi-tracks. When a semi-track is etched, the etchant travels further parallel to the c-axis than perpendicular to it, producing a thin knife blade shape for the etched semi-track (Gleadow 1981). Thus a potential host semi-track presents a wider face to the direction perpendicular to the c-axis, and this favours the sampling of tints at high angles ϕ. Note that this orientation bias is a consequence of anisotropic etching.

We will look at this more closely. If $N(\phi)$ is the number of horizontal tints at angle ϕ, then, to a first approximation

$$\mathrm{E}[N(\phi)] \propto \{a \sin\phi + b \cos\phi\}\, \mu(\phi),$$

where $\mu(\phi)$ is the true mean length of tracks at angle ϕ (figure 8). Measurements on etched openings of semi-tracks on a prismatic face of a fluorapatite suggest that $a/b \approx 3.7$, although within the crystal this ratio may be slightly different. Table 4 gives fitted frequencies and standardized residuals assuming $a/b = 3.7$ and

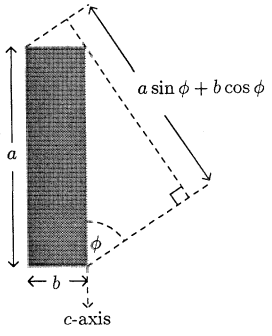

Figure 8. Idealized horizontal cross-section of an etched semi-track. It is rectangular with the a dimension parallel to the c-axis and about 3.5 to 4 times longer than the b dimension. To a potential tint at angle ϕ it presents a face of width $a \sin\phi + b \cos\phi$.

Table 3[a]. *Numbers of horizontal tints*

	ϕ/deg						
temperature/°C	0–15	16–30	31–45	46–60	61–75	76–90	total
u.c.[b]	5	18	31	42	55	49	200
260	10	23	26	50	47	44	200
310	7	22	36	54	44	39	202
336	8	24	40	55	41	32	200
352	2	17	24	31	27	17	118

[a] Data from Green *et al.* (1986), 50 s etching time.
[b] Unannealed control.

Table 4. *Further analysis of data of table* 3

temperature/°C	ϕ/deg 0–15	16–30	31–45	46–60	61–75	76–90
			fitted frequencies			
u.c.[a]	16.63	26.33	34.12	39.43	41.95	41.54
260	16.95	26.76	34.47	39.51	41.60	40.71
310	17.55	27.60	35.29	40.02	41.55	39.99
336	18.60	28.95	36.29	39.93	39.81	36.42
352	15.54	23.16	26.45	24.70	18.52	9.64
			standardized residuals			
u.c.[a]	−2.48	−1.31	−0.42	0.32	1.53	0.89
260	−1.35	−0.57	−1.17	1.26	0.65	0.40
310	−2.12	−0.84	0.09	1.66	0.30	−0.12
336	−2.06	−0.73	0.47	1.78	0.15	−0.59
352	−3.29	−1.06	−0.39	0.97	1.42	1.58

[a] Unannealed control

$\mu(\phi) = \eta + \xi \cos\phi$, where at each temperature η and ξ were estimated from the measured lengths and angles, using the method described below equation (9).

The model fails to explain the data completely, particularly at low angles where too few tracks are seen, but it does explain much of the broad pattern. Excluding angles below 30° and refitting the model produces a good fit. This paucity of tints at a low angle to the c-axis is commonly encountered by observers in routine work, virtually all of which is unpublished. Whether the correct explanation lies in a further sampling bias, an etching effect or some other effect is unknown.

For unannealed samples orientation bias should not affect the observed length distribution, as l does not depend on ϕ. But for annealed samples, it could do; thus for tints, orientation bias favours tracks at a high angle ϕ. These tracks are relatively short, so orientation bias acts in the opposite direction to length bias. For tincles, the angular distribution will depart from uniform if host fractures tend to run in a particular direction and this could be reflected in the measured lengths. A simple way to correct for orientation bias is to measure the angle ϕ between each horizontal track and the c-axis, and standardize all distributions to have a common distribution for ϕ (usually the uniform distribution would be chosen). If standardization by ϕ is not used, it would at least be wise to separate tints from tincles when measuring confined track lengths.

Calculation of mean tint length and mean tincle length in routine work reveals that the latter is slightly greater in general, particularly in annealed samples: this is a consequence, at least partly, of observed differences in orientation bias between tints and tincles, but it could also be attributed to fracture-thickness bias in sampling tincles, which we discuss next. Anisotropic etching implies that fractures at a high-angle to the c-axis will tend to be wider, and this is also seen in practice.

4.3. *Fracture-thickness bias*

In §4.1.1 we saw that tincles are subject to 'fracture-thickness' bias, in which longer tracks intersecting a fracture have a higher probability of having both ends exposed, and hence of being measured. A similar bias favours tracks at a high angle to the fracture. In some extreme cases, very short tracks may be hidden in wider

fractures. We now consider a non-parametric method for estimating the anisotropic length distribution from measurements on tincles.

Consider only horizontal tracks at angle ϕ to the c-axis. Let τ_ϕ be the concentration of fissioned uranium atoms associated with these, and let F_ϕ and f_ϕ be their length distribution and density function. A track of length l' crossing a fracture of thickness β at angle ψ will have length $l'-\beta/\sin\psi$ outside the fracture, so that the number of such tracks sampled will be proportional to this quantity. If there are m fractures, the kth of which has thickness β_k and angle of intersection ψ_k, then the expected number of tincles longer than l is

$$\mathrm{E}[N_\phi(l)] = \tau_\phi \sum_{k=1}^{m} C_k \int_{\beta_k/\sin\psi_k}^{\infty} I_{\{l'>l\}}(l'-\beta_k/\sin\psi_k) f_\phi(l')\,\mathrm{d}l',$$

where C_k is the effective area of the kth fracture to intersection, and where it is convenient to use the indicator function $I_{\{l'>l\}} = 1$ if $l' > l$ (0 otherwise). The quantities C_k are not measurable, but can be weighted out as follows.

If we assign weight $(l'-\beta_k/\sin\psi_k)^{-1}$ to a track of length l' crossing the kth fracture, then the expected total weight associated with tincles longer than l is

$$\mathrm{E}[W_\phi(l)] = \tau_\phi \sum_{k=1}^{m} C_k \int_{\beta_k/\sin\psi_k}^{\infty} I_{\{l'>l\}} f_\phi(l')\,\mathrm{d}l' = \tau_\phi \sum_{k=1}^{m} C_k[1-F_\phi(\max\{l, \beta_k/\sin\psi_k\})].$$

Label the fractures so that $\beta_k/\sin\psi_k$ increases with k and suppose firstly that $F_\phi(\beta_m/\sin\psi_m) = 0$. Then

$$\mathrm{E}[W_\phi(l)]/\mathrm{E}(W_\phi(0)] = 1-F_\phi(l)$$

and we may estimate $1-F_\phi(l)$ by the proportion of the total weight in the sample associated with tincles longer than l. Explicitly this is

$$1-\hat{F}_\phi(l) = \frac{\sum_{k=1}^{m}\sum_{j=1}^{n_k} I_{\{l_{jk}>l\}}(l_{jk}-\beta_k/\sin\psi_k)^{-1}}{\sum_{k=1}^{m}\sum_{j=1}^{n_k}(l_{jk}-\beta_k/\sin\psi_k)^{-1}},$$

where n_k is the number of tracks (at angle ϕ) measured in the kth fracture and l_{jk} is the length of the jth track in the kth fracture. When all $\beta_k = 0$, this reduces to the usual non-parametric formula (Cox 1969, equation (5.6)) for estimating a distribution function from length-biased data.

In practice, the assumption that $F_\phi(\beta_m/\sin\psi_m) = 0$ may not hold. Suppose at least that $F_\phi(\beta_1/\sin\psi_1) = 0$. Temporarily write $w_{jk} = (l_{jk}-\beta_k/\sin\psi_k)^{-1}$ and $u_k = \beta_k/\sin\psi_k$ (with $u_0 = 0$ and $u_{m+1} = \infty$) so that $\hat{F}_\phi(u_1) = 0$. Then an extension of the above argument leads to the natural estimator of the conditional probability that the true length of a track exceeds l given that it exceeds u_i, namely

$$\frac{1-\hat{F}_\phi(l)}{1-\hat{F}_\phi(u_i)} = \frac{\sum_{k=1}^{i}\sum_{j=1}^{n_k} I_{\{l_{jk}>l\}} w_{jk}}{\sum_{k=1}^{i}\sum_{j=1}^{n_k} I_{\{l_{jk}>u_i\}} w_{jk}} \equiv s_i(l\,|\,u_i), \quad u_i < l \leqslant u_{i+1}, \quad i = 1, 2, \ldots, m,$$

so that

$$1-\hat{F}_\phi(l) = s_i(l\,|\,u_i)\prod_{j=0}^{i-1} s_j(u_{j+1}\,|\,u_j),$$

with $s_0(u_1 \mid u_0) = 1$. Despite their elegance, these estimators suffer from the types of problems discussed by Watson (1971), essentially because $x^{-1} \to \infty$ as $x \to 0$. For the purpose of estimating geological parameters it would seem better to assume a parametric form for F_ϕ.

5. Estimation using projected semi-track measurements

In this section, we are concerned with estimating geological parameters from measurements of lengths and angles of projected semi-tracks. We concentrate on the important problem of a two-component mixture, described in §3.3.

Using the anisotropic line-segment model described in §3.2, Galbraith & Laslett (1988) showed that the joint density function of r and ω (figure 2) is

$$f_{\mathrm{ps}}(r, \omega) = \sec\omega \int_{\omega}^{\frac{1}{2}\pi} \sin\phi \left\{1 - F_\phi\left(\frac{r\cos\omega}{\cos\phi}\right)\right\} \mathrm{d}\phi \Big/ \int_0^{\frac{1}{2}\pi} \sin^2\phi \mathrm{E}[l \mid \phi]\, \mathrm{d}\phi$$

$$(r > 0, 0 < \omega < \tfrac{1}{2}\pi), \quad (7)$$

where F_ϕ is the conditional distribution function of l given ϕ. We further assume that for a set of tracks all annealed to the same extent, and that are fully etched (non-gapped), F_ϕ is normal with variance σ_0^2 and mean

$$\mathrm{E}[l \mid \phi] = \eta + \xi\cos\phi. \quad (8)$$

So $f_{\mathrm{ps}}(r, \omega)$ has three parameters σ_0, η, ξ, which we reduce to one unknown parameter by treating $\sigma_0 = 0.99$ as known from past data, and by assuming a relation

$$\xi = 1.461 - 0.513(\eta - 10) + 0.331\,[(\eta - 10)^2 + 1]^{\frac{1}{2}}, \quad (9)$$

which closely describes estimated (η, ξ) pairs from 13 previous annealing studies of confined tracks in Durango apatite. (In each study, η and ξ were estimated by maximum likelihood using the normal distribution of l given ϕ truncated at $b_0 + b_1\cos\phi$, where b_0 and b_1 were chosen so that all gapped tracks were excluded. The length-bias correction for observed lengths at each angle ϕ was found to be minuscule. In excluding the gapped tracks, we are assuming that semi-tracks are fully etched (non-gapped). Note that semi-tracks are directly etched from the surface, whereas confined tracks require the etchant to travel further. The etch time and acid strength of the etchant have been arrived at by observing when the track density on a prismatic face becomes stable in real (annealed) samples, suggesting that significant gapping of semi-tracks is unlikely to be present. An approach making fewer parametric assumptions is possible, but would require very careful treatment of geometrical sampling biases.)

We report the results in terms of the parameter

$$\mu = \frac{2}{\pi}\int_0^{\frac{1}{2}\pi} (\eta + \xi\cos\phi)\, \mathrm{d}\phi = \eta + 2\xi/\pi,$$

which is the true mean track length standardized with respect to a uniform distribution of ϕ. Thus, for a single cohort of tracks, the joint distribution of (l, ϕ), and hence of (r, ω), is specified by μ.

Now consider a sample comprising a cohort of lightly annealed tracks with mean

length parameter μ_0 mixed with a cohort of more heavily annealed tracks with parameter $\mu_1 < \mu_0$. Then

$$F_\phi(l) = (1-p)\,F_{\phi 0}(l) + pF_{\phi 1}(l). \tag{10}$$

In the context of figure 5, p would correspond to the true proportion of tracks formed prior to uplift, and would not depend on ϕ, while μ_0 and μ_1 reflect the current and maximum temperature respectively. We want to estimate p, μ_0 and μ_1 from data on r and ω.

Our estimation method is as follows. We group r and ω into 1 μm × 10° groups $\{\Omega_g\}$, and work with the frequency data $\{n_g\}$, where n_g is the number of tracks in Ω_g. The log likelihood is

$$\mathscr{L} \equiv \sum_g n_g \ln p_g, \tag{11}$$

where
$$p_g \equiv \Pr\{(r,\omega) \in \Omega_g\} = \frac{(1-p)\,J(g;F_{\phi 0}) + pJ(g;F_{\phi 1})}{(1-p)\sum_g J(g;F_{\phi 0}) + p\sum_g J(g;F_{\phi 1})}$$

and
$$J(g;F_\phi) = \int_{\Omega_g} \mathrm{d}r \frac{\mathrm{d}\omega}{\cos\omega} \int_\omega^{\frac{1}{2}\pi} \sin\phi \left[1 - F_\phi\left(\frac{r\cos\omega}{\cos\phi}\right)\right] \mathrm{d}\phi.$$

To maximize (11) efficiently, $J(g, F_{\phi 0})$ and $J(g, F_{\phi 1})$ were computed and stored for each g and each μ_0 and μ_1 on the grid $\{8.0, 8.5, \ldots, 16.5\ \mu\mathrm{m}\}$. Once these quantities are stored, the log likelihood (11) can be maximized over the space

$$\mu_0 = 8.0, 8.5, \ldots, 16.5; \quad \mu_1 = 8.0, 8.5, \ldots, \mu_0 - 0.5 \quad (0 \leqslant p \leqslant 1)$$

in less than a minute for any new data-set. Then the maximum likelihood estimates and observed information matrix can be computed by interpolation. Comparisons between this procedure, and a direct maximization of (11) using IMSL optimization routines, showed that not only was it much more efficient, but also more reliable, particularly when $\hat{p}$ was near 0 or 1.

The method was tested on simulated data sets of 500 (r, ω) pairs. For μ_0 fixed, the log likelihood had a very clear maximum with respect to p and μ_1, but μ_0 itself was poorly determined. In practice this may not matter, because a good estimate of μ_0 can often be obtained from knowledge of the geology and the current thermal environment. Henceforth we assume μ_0 known.

Simulation studies for fixed μ_0 showed that good estimates of μ_1 and p may be obtained when p is greater than about 0.6. This suggests that projected semi-track measurements may only reliably be used to detect a 'recent' thermal event, since p relates to the timing of the thermal event, and μ_1 to its severity. If a thermal event occurs before the half-way mark of the mineral's lifetime, the estimation procedure will sometimes confuse this with a milder thermal event that occurred much later (e.g. $p = 0.4$, $\mu_1 = 9.0$, is estimated as $\hat{p} = 0.8$, $\hat{\mu}_1 = 12.5$ say). For the purposes of making a geological interpretation, such a confusion could be disastrous. However, the size of the confidence limits in such a case should offer some protection.

The method was then applied to the experiments D6, D10, D15, D17, D19 and D21 described in §4.1.2; about 500 (r, ω) pairs were measured in each. Figure 9 displays the data for the mixture D21 and the corresponding controls. The unannealed and the annealed controls are readily distinguishable. Furthermore, the mixture (D21) nearly matches the pattern in the annealed control, apart from a few 'long' projected tracks at high angles that betray the presence of the unannealed component. The

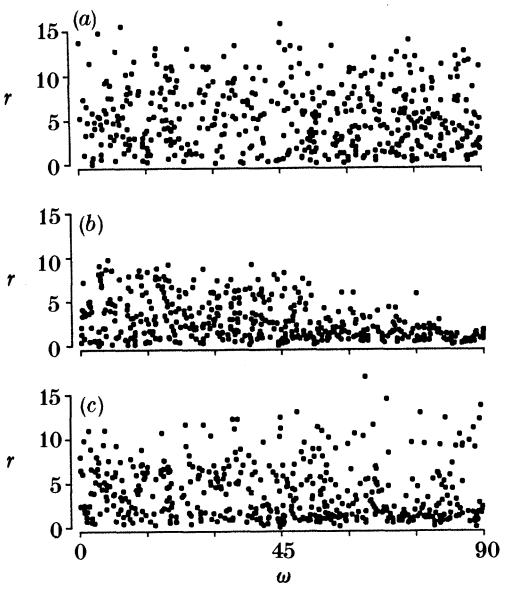

Figure 9. Projected semi-track data for three experiments: (*a*) D13, an unannealed control sample, (*b*) D19, a heavily annealed control sample, and (*c*) D21, a mixture of unannealed and annealed tracks. Here r is the projected length (in micrometres) of a semi-track onto the prismatic face of an apatite crystal, and ω is the angle (in degrees) of this projection to the c-axis. About 500 semi-tracks were measured in each experiment.

Table 5. *Comparison of estimated and true* p, μ_1

experiment	p	$\hat{p}$	SE	μ_1	$\hat{\mu}_1$	SE
D17	0.833	0.901	0.047	10.27	10.46	0.52
D21	0.833	0.766	0.037	8.97	8.04	0.49
D6	0.938	0.816	0.029	10.27	9.37	0.43
D10	0.938	0.929	0.020	8.97	8.01	0.47
D15	1.000	1.000	—	10.27	9.81	0.46
D19	1.000	1.000	—	8.97	8.00	—

measurement of ω in addition to r is clearly informative. Comparison of figure 9 with figure 4, which shows the confined track data for D21, illustrates how much more information is contained in the confined track measurements.

Table 5 gives estimates of p and μ_1 for each experiment, compared with the true values, when μ_0 is fixed at 16 μm. It is clear that the procedure works for real measurements at least approximately, although on this limited evidence $\hat{\mu}_1$ slightly underestimates μ_1. The nominal true values are themselves estimates, μ_1 being estimated directly from confined track data for the annealed controls by omitting the very-short gapped tracks, which may partly account for the discrepancy. But perhaps a more plausible explanation lies in the dynamics of the etching process: the confined tracks become longer with increasing etch time, because of bulk etching of host material at each end of a confined track. This applies also to semi-tracks, but at the same time the surface is etched away, which may counterbalance the etching of the ends of the semi-tracks to some extent. Sequential etching experiments are required to quantify these effects, but, from a practical viewpoint, they are

secondary. A more serious potential problem is the reliance of the estimation procedure on the relatively-few long projected lengths at high angles to the c-axis. In small samples, these could easily be missing by chance, or only sparsely represented, and the presence of the long component may not be detected.

6. Combined likelihood for a two-component mixture

Although it has been recognized (Gleadow *et al.* 1986; Green *et al.* 1989) that proper interpretation of apatite fission track data should combine information from both measured ages (track counts) and lengths, no formal analysis of the complete data has been presented in the literature. Here we discuss the feasibility of using the joint likelihood of all counts, lengths and orientations for the case of a two-component mixture.

Routine fission track dating uses equation (5) to estimate the 'age' t of a crystal; usually interpreted as the time since rapid cooling shortly after its formation. But for the more complex history described in §3.3, we could try to estimate, simultaneously with t, the time t_u and maximum temperature T_u at uplift. We saw that a crystal experiencing this history contains (to a good approximation) a two-component mixture of tracks: a proportion p formed before uplift, having mean length μ_1 and a proportion $1-p$ formed subsequently, having mean length μ_0. We use the parametrization introduced in §5.

Now μ_0 will be known from the current temperature and if we estimate μ_1 we can infer T_u. Also from (1)

$$p = \frac{p(t_u)}{p(t)} = \frac{1-\exp[-(\lambda+\lambda_f)t_u]}{1-\exp[-(\lambda+\lambda_f)t]},$$

so if we estimate t and p we can infer t_u.

Consider data from a single crystal with exposed area A. We count n_s spontaneous tracks intersecting A and n_i induced tracks intersecting the corresponding area of the mica. From §2, n_s and n_i have independent Poisson distributions and their joint likelihood is

$$\exp\{-A\rho_s\}\frac{(A\rho_s)^{n_s}}{n_s!}\exp\{-A\rho_i\}\frac{(A\rho_i)^{n_i}}{n_i!} \tag{12}$$

with $$\rho_s = \frac{1}{2}\frac{\lambda_f}{\lambda+\lambda_f}[e^{(\lambda+\lambda_f)t}-1]\tau_c\mu^*, \quad \rho_i = \tfrac{1}{4}\Phi\sigma\beta\tau_c\mu_i,$$

where $$\mu^* = \frac{4}{\pi}[(1-p)(\tfrac{1}{2}\eta_0+\tfrac{1}{3}\xi_0)+p(\tfrac{1}{2}\eta_1+\tfrac{1}{3}\xi_1)].$$

Here we have used equations (2) and (6) with

$$E[l\,|\,\phi] = (1-p)(\eta_0+\xi_0\cos\phi)+p(\eta_1+\xi_1\cos\phi).$$

Note that μ^*, satisfying $\rho_s = \frac{1}{2}\tau\mu^*$, is the 'equivalent isotropic length' giving rise to the density ρ_s. Expressing ρ_s/ρ_i in terms of t gives, analogously to (5),

$$t = \frac{1}{\lambda+\lambda_f}\ln\left\{1+\frac{\lambda+\lambda_f}{2\lambda_f}\beta\sigma\Phi\frac{\mu_i}{\mu^*}\frac{\rho_s}{\rho_i}\right\}. \tag{13}$$

The parameters t, p and μ_1 are not identifiable from (12) without further information,

and there is an extra nuisance parameter τ_c. (Indeed the purpose of counting n_i is to measure τ_c. It is sometimes convenient to eliminate τ_c by using just the conditional likelihood of n_s given n_s+n_i. The fluence Φ is measured as described in §2 and μ_i will be known from extensive measurements on laboratory induced tracks.)

Now suppose the projected semi-track lengths and angles (r, ω) have been measured for the n_s spontaneous tracks. Then the likelihood (12) would be multiplied by

$$\prod_{j=1}^{n_s} f_{ps}(r_j, \omega_j), \tag{14}$$

where f_{ps} is given by (7). Since f_{ps} does not depend on t, we can estimate p and μ_1 by maximizing (14), for example as in §5, and then obtain the maximum likelihood estimate of t from (13) by substituting n_s/n_i in place of ρ_s/ρ_i.

Suppose also that there are n_t tints intersecting the semi-tracks and their lengths and angles (l, ϕ) have been measured. The distribution of n_t and ϕ depends on a better understanding of orientation bias than has been achieved in §4.2, so although these measurements contain relevant information, it seems safer to use just the likelihood from the conditional distribution of length given orientation of sampled tints. This is

$$\prod_{j=1}^{n_t} \frac{l_j f_{\phi_j}(l_j)}{\mathrm{E}[l \mid \phi_j]}, \tag{15}$$

where f_ϕ is the density corresponding to F_ϕ in (10).

Similar considerations apply to tincles. The probability of sampling a tincle of a particular length and orientation depends on the number, orientations and sizes of the fractures in the crystal. It is therefore important to measure these for the actual host fractures and condition on them to avoid terms involving unknown or unmeasurable quantities (cf. §4.3). Thus if (l, ϕ, β, ψ) is measured for each of n_c tincles, the conditional likelihood of the lengths given the other measurements is

$$\prod_{j=1}^{n_c} \frac{(l_j - \beta_j/\sin\psi_j) f_{\phi_j}(l_j)}{\int_{\beta_j/\sin\psi_j}^{\infty} (l - \beta_j/\sin\psi_j) f_{\phi_j}(l)\,\mathrm{d}l}. \tag{16}$$

Thus t, p and μ_1 can be estimated by maximizing the product of (12), (14), (15) and (16). As t only appears in (12), p and μ_1 are estimated from the last three terms and then t is estimated from (13) by substituting n_s/n_i in place of ρ_s/ρ_i.

We conclude from §4 and §5 that (14), (15) and (16) can be used with some confidence, possibly with minor modifications as we learn more about the etching dynamics, and in §5 we have gained a good idea of the sort of information that projected semi-track lengths and angles can provide. It is not clear how much the precisions of the estimates could be improved by including terms from the distributions of n_t and ϕ, but for the sake of robustness it seems best to exclude them at present. Of course there are practical advantages in treating even the above terms separately, at least initially, to check that they agree or otherwise assess goodness of fit, and to keep the analysis simple so that other variables, such as chemical composition and depth of sample down the borehole, can more easily be incorporated.

R.F.G. received financial assistance from CSIRO to visit Melbourne during preparation of this article.

References

Cox, D. R. 1969 Some sampling problems in technology. In *New developments in survey sampling* (ed. N. Johnson & H. Smith), pp. 506–527. New York: Wiley.

Dakowski, M. 1978 Length distributions of fission tracks in thick crystals. *Nucl. Track Detection* **2**, 181–190.

Duddy, I. R., Green, P. F. & Laslett, G. M. 1988 Thermal annealing of fission tracks in apatite, 3. Variable temperature annealing. *Chem. Geol.* **73**, 25–38.

Galbraith, R. F. 1984 On statistical estimation in fission track dating. *J. math. Geol.* **16**, 653–669.

Galbraith, R. F. 1988 Graphical display of estimates having differing standard errors. *Technometrics* **30**, 271–281.

Galbraith, R. F. & Laslett, G. M. 1988 Some calculations relevant to thermal annealing of fission tracks in apatite. *Proc. R. Soc. Lond.* A **419**, 305–321.

Gleadow, A. J. W. 1981 Fission track dating methods: what are the real alternatives? *Nucl. Tracks* **5**, 3–14.

Gleadow, A. J. W. & Duddy, I. R. 1981 A natural long term annealing experiment for apatite. *Nucl. Tracks* **5**, 169–174.

Gleadow, A. J. W., Duddy, I. R., Green, P. F. & Lovering, J. F. 1986 Confined fission track lengths in apatite: a diagnostic tool for thermal history analysis. *Contrib. Mineral. Petrol.* **94**, 405–415.

Green, P. F. 1981 'Track-in-track' length measurements in annealed apatites. *Nucl. Tracks* **5**, 121–128.

Green, P. F. & Durrani, S. A. 1977 Annealing studies of tracks in crystals. *Nucl. Tracks* **1**, 33–39.

Green, P. F., Duddy, I. R., Gleadow, A. J. W., Tingate, P. R. & Laslett, G. M. 1986 Thermal annealing of fission tracks in apatite, 1. A qualitative description. *Chem. Geol.* **59**, 237–253.

Green, P. F., Duddy, I. R., Laslett, G. M., Hegarty, K. A., Gleadow, A. J. W. & Lovering, J. F. 1989 Thermal annealing of fission tracks in apatite, 4. Quantitative modelling techniques and extension to geological timescales. *Chem. Geol.* **79**, 155–182.

Hurford, A. J. & Green, P. F. 1983 The zeta age calibration of fission-track dating. *Isotope Geosci.* **1**, 285–317.

Laslett, G. M., Gleadow, A. J. W. & Duddy, I. R. 1984 The relationship between fission track length and track density in apatite. *Nucl. Tracks* **9**, 29–38.

Laslett, G. M., Green, P. F., Duddy, I. R. & Gleadow, A. J. W. 1987 Thermal annealing of fission tracks in apatite, 2. A quantitative analysis. *Chem. Geol.* **65**, 1–13.

Laslett, G. M., Kendall, W. S., Gleadow, A. J. W. & Duddy, I. R. 1982 Bias in measurement of fission track length distributions. *Nucl. Tracks* **6**, 79–85.

Price, P. B. & Walker, R. M. 1963 Fossil tracks of charged particles in mica and the age of minerals. *J. geophys. Res.* **68**, 4847–4862.

Storzer, D. & Wagner, G. A. 1969 Correction of thermally lowered fission track ages of tektites. *Earth planet. Sci. Lett.* **5**, 463–468.

Watson, G. S. 1971 Estimating functionals of particle size distributions. *Biometrika* **58**, 483–490.

PHILOSOPHICAL TRANSACTIONS OF THE ROYAL SOCIETY A MATHEMATICAL, PHYSICAL & ENGINEERING SCIENCES

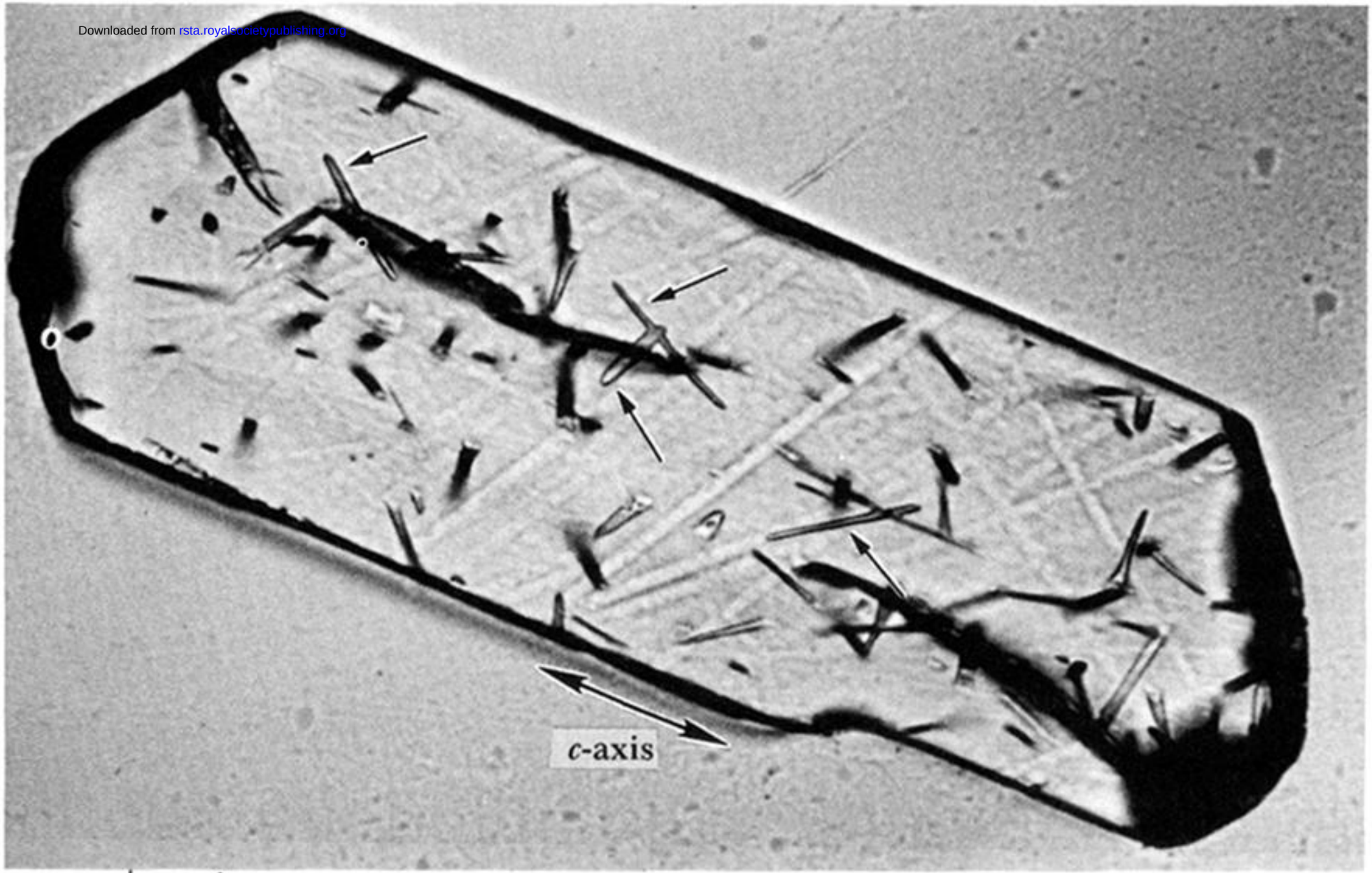

igure 1. Fission tracks in apatite. Tracks intersecting a polished surface (i.e. semi-tracks) are vealed by chemical etching. The track openings are seen as light-coloured rectangular slots, and e aligned in the direction of the crystal's '*c*-axis'. Four totally confined tracks, indicated by rows, have been etched because they intersect semi-tracks or fractures. The larger etched regions e fractures; the faint lines are polishing scratches. Photograph reproduced, with permission, from leadow *et al.* (1986).